

The single-particle space-momentum angle distribution effect on two-pion HBT correlation with the Coulomb interaction

Hang Yang, Qichun Feng, Yanyv Ren, Jingbo Zhang*, Lei Huo

School of Physics, Harbin Institute of Technology, Harbin 150001, China

E-mail: jinux@hit.edu.cn

Abstract. We calculate the HBT radius R_s for π^+ particles with the Coulomb interaction by using the string melting version of a multiphase transport(AMPT) model. Then we study the single-particle space-momentum angle distribution on the transverse plane and build the numerical connection between this distribution and the transverse momentum dependence of R_s . Additionally, we study the Coulomb interaction effect on this numerical connection.

Keywords: HBT Radii, Transverse Momentum Dependence, Space-Momentum Angle Distribution, AMPT

1. Introduction

The Hanbury-Brown Twiss (HBT) method is a useful tool in relativistic heavy ion collisions, and it can probe the dynamically generated geometry structure of the emitting system. It is also named two-pion interferometry method, for it is often used with the pion particles which are the most particles in the high energy collisions. The method of measuring the photons correlation to extract angular sizes of stars was invented by Hanbury Brown and Twiss in astronomy in the 1950s[1]. Several years later, this method was extended in $\bar{p} + p$ collisions by G. Goldhaber, S. Goldhaber, W. Lee and A. Pais[2]. After years of improvement, the HBT method becomes a precision tool for measuring space-time and dynamic properties of the emitting source[3, 4, 5], and it has been used in $e^+ + e^-$, hadron+hadron, and heavy ion collisions[6, 7, 8].

At the high energies of the heavy-ion collisions, the normal state matter transform to the Quark-Gluon Plasma(QGP) which is a new state matter consisting of deconfined quarks and gluons[9, 10]. There are two kinds of phase transition between the low-temperature hadronic phase and the high-temperature quark-gluon plasma phase, cross-over transition and first-order transition. And the critical end point(CEP) is the point where the first-order phase transition terminates[11, 12]. Searching for the CEP at lower energies on the QCD phase diagram is one main goal of the Beam Energy Scan(BES) program[13, 14]. There will be critical behavior near the CEP[15], and the transport coefficients will change violently, which will lead the changes in HBT radii, so the CEP can be estimated by the HBT analysis[16, 17].

The space-momentum correlation is important in HBT research, it is caused by the collective expanding behavior of the collision source[18]. And this space-momentum correlation can lead to the changing of the HBT radii with the transverse momentum of the pion pairs[19]. This phenomenon is named the transverse momentum dependence of HBT radii. Our research is focusing on the connection between the space-momentum correlation and this phenomenon. We need a tool to quantify this space-momentum correlation, so we introduce the normalized single-particle space-momentum angle distribution[20, 21]. This distribution consists of a series of angles belonging to freeze-out pions in the same energy sections and the same transverse momentum pion pair sections. We use the projection angle $\Delta\theta$ on the transverse plane in our study, as shown in Figure 1. With this angle distribution, we can obtain more information about the source from the transverse momentum dependence of HBT radii.

In our previous work, we treated three kinds of pions as one, considered them to have the same mass, and neglected the Coulomb interaction[20, 21]. While in experiments, the three kinds of pions can be distinguished and the charged ones are more easily to be detected. The π^+ and π^- are basic same, so in this paper, we only focus on the π^+ and discuss the influence of the Coulomb interaction on the numerical connection between the single-particle space-momentum angle $\Delta\theta$ distribution and the transverse momentum dependence of HBT radius R_s . We use a multiphase transport (AMPT) model to generate the freeze-out π^+ particles at different collision energies. This model

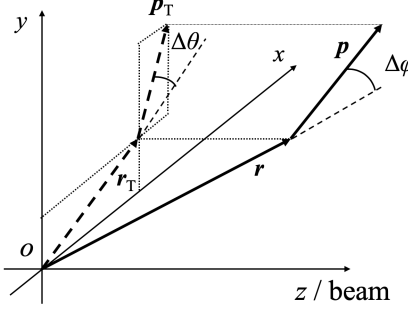


Figure 1. The diagram of the $\Delta\varphi$ and $\Delta\theta$. $\Delta\varphi$ is the angle between \mathbf{r} and \mathbf{p} , and $\Delta\theta$ is the angle between \mathbf{r}_T and \mathbf{p}_T , at the freeze-out time. The origin is the center of the source.

contains the physical processes of the relativistic heavy-ion collisions[22] and has already been widely used in HBT researches[23, 24, 25].

The paper is organized as follows. In Sec. II, the string melting AMPT model and the HBT correlation are briefly introduced. In Sec. III, the HBT radius R_s for π^+ particles are calculated in two conditions, with and without the Coulomb interaction. In Sec. IV, we discuss the influence of the single-particle space-momentum angle $\Delta\theta$ distribution on the HBT radius R_s , and we build the numerical connections between them with and without the Coulomb interaction. In final Section, we give the summary.

2. The string melting AMPT model and methodology

In this paper, we use the string melting AMPT model, this version can give a better description for the correlation function in HBT researches[22, 26]. The string melting AMPT model contains four main parts. The first part uses the HIJING model to produce the partons and strings, and the strings will fragment into partons. In the second part, using Zhang's parton-cascade(ZPC) model to describe the interactions among these partons. Then in the third part, a quark coalescence model is used to combine these partons into hadrons. In the last part, these hadrons interaction till hadrons freeze-out is described by a relativistic transport(ART) model. With the models in these four main parts, the string melting AMPT model can describe the heavy-ion collisions includes the transitions and the interactions.

The HBT radii are important in HBT research, they can be extracted by the HBT three-dimensional correlation function, the normal form can be written as[27]

$$C(\mathbf{q}, \mathbf{K}) = 1 + \lambda e^{-q_o^2 R_o^2(\mathbf{K}) - q_s^2 R_s^2(\mathbf{K}) - q_l^2 R_l^2(\mathbf{K}) - 2q_o q_l R_{ol}^2(\mathbf{K})}, \quad (1)$$

and in this paper, we also use the form with the Coulomb interaction as[28]

$$C(\mathbf{q}, \mathbf{K}) = 1 - \lambda + \lambda K_{coul} [1 + e^{-q_o^2 R_o^2(\mathbf{K}) - q_s^2 R_s^2(\mathbf{K}) - q_l^2 R_l^2(\mathbf{K}) - 2q_o q_l R_{ol}^2(\mathbf{K})}], \quad (2)$$

where $\mathbf{q} = \mathbf{p}_1 - \mathbf{p}_2$, $\mathbf{K} = (\mathbf{p}_1 + \mathbf{p}_2)/2$, C is the two pion correlation, K_{coul} is the squared Coulomb wave function, and the λ is the coherence parameter. R is for the

HBT radius. It is usually used in the ‘out-side-long’ coordinate system, this system is used for the pair particles, as shown in Figure 2. The *l* is the longitudinal direction, it is also the beam direction. The *o* and *s* are outward and sideward directions defined on the transverse plane. The pair particles momentum direction is defined as the outward direction, so the side direction is the direction perpendicular to the outward direction. The R_{ol} is the cross term, it will vanish at mid-rapidity in a symmetric system. For that reason, we set the biggest impact parameter as 1.4 fm, and chose mid-rapidity range $-0.5 < \eta < 0.5$. We use Equation 1 to fit the correlation without the Coulomb interaction and use Equation 2 to fit the correlation with the Coulomb interaction.

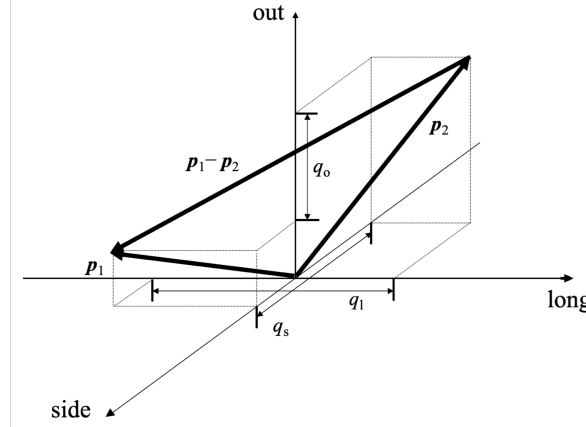


Figure 2. The diagram of ‘out-side-long’(o-s-l) coordinate system.

We use the Correlation After Burner (CRAB) code to generate the correlation, it can read the phase space information from the string melting AMPT model[29]. It generates the correlation by the formula

$$C(\mathbf{q}, \mathbf{K}) = 1 + \frac{\int d^4x_1 d^4x_2 S_1(x_1, \mathbf{p}_2) S_2(x_2, \mathbf{p}_2) |\psi_{\text{rel}}|^2}{\int d^4x_1 d^4x_2 S_1(x_1, \mathbf{p}_2) S_2(x_2, \mathbf{p}_2)}, \quad (3)$$

where ψ_{rel} is the relative two particles wave function which include the interaction between two particles. $S(x, \mathbf{p})$ is the single particle emission function.

3. The Coulomb effect on R_s

We produced the particles of Au+Au collisions at $\sqrt{S_{NN}} = 14.5, 19.6, 27, 39, 62.4, 200$ GeV by the string melting AMPT model. These energies are the BES energies, each energy has more than forty thousand collision events. We separate the pair transverse momentum 125–625 MeV/c into 9 bins. For the last bin that has fewer particles, we set it for 525–625 MeV/c, the width is twice than others. Then we use the CRAB code to calculate the correlation functions for the π^+ particles. The Coulomb interaction can change the correlation functions, which are shown in Figure 3. If neglect the Coulomb interaction, because of the collective flow created by the collisions, two π^+ particles

are easily frozen out along the same direction, and the correlation function will be a Gaussian form. While considering the Coulomb interaction, the two π^+ particles have the Coulomb potential between them, and it will change the two π^+ wave function ψ_{rel} . The closer of the two π^+ , the bigger the Coulomb potential between them. When two π^+ are close to each other, the probability density of the two π^+ will decrease, and it will cause the decrease of the Correlation function at the direction along the momentum difference direction. q_s is related to the momentum difference on the transverse plane, so there is a little gap of the correlation function on the q_s direction.

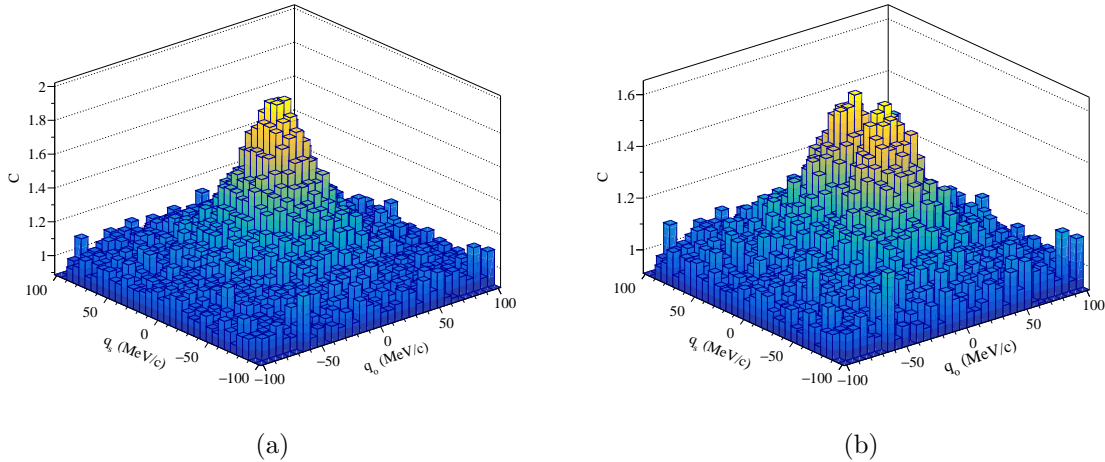


Figure 3. Correlation functions of π^+ in the q_o and q_s directions, generated by the string melting AMPT model for the Au+Au collisions at $\sqrt{S_{NN}} = 200$ GeV. The K_T range is 325–375 MeV/c, and the q_l range is -3–3 MeV/c. Figure (a) neglects the Coulomb interaction, and figure (b) is the situation with the Coulomb interaction.

We only focus on the HBT radius R_s , it is least affected by other physical factors and related to the transverse size of the source[30]. The transverse momentum dependence of R_s with and without Coulomb interaction is shown in Figure 4. The obvious difference is the values of R_s calculated with the Coulomb interaction are smaller than those without the Coulomb interaction at small pair momentum. The strengths of K_T dependence of R_s , especially for the lower collision energies, can barely be distinguished. And it is even worse for the situation with the Coulomb interaction. So we introduced a parameter b which can describe the strength of K_T dependence of R_s . And it is in the fit function

$$R = aK_T^b, \quad (4)$$

where parameter a is just a common constant.

The parameter b can be used to describe the strength for the transverse momentum dependence of R_s , as shown in Figure 5. All the $|b|$ values increase with increasing collision energy, which means that, at higher collision energies, the values of R_s will change more violently with the transverse pair momenta. The dots for all pions are taken from our last work, which treated all pions as one kind and generated with

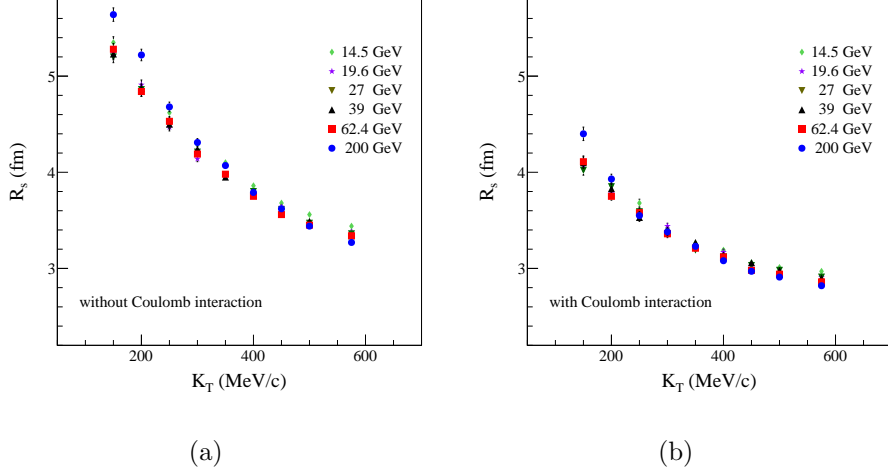


Figure 4. Transverse momentum dependence of R_s in AMPT model.

the 0 fm collision parameter[21]. And their values are close to the π^+ without the Coulomb interaction. It indicates the kind of pions have a little change on the strength for the transverse momentum dependence of R_s . The $|b|$ values are smaller with the Coulomb interaction, which means the Coulomb interaction inhibits the strength of the transverse momentum dependence of HBT radii. Furthermore, with increasing the collision energies, the differences of the b values for π^+ between the two situations are also increased, which indicates this inhibition is stronger at high collision energies for the Coulomb interaction.

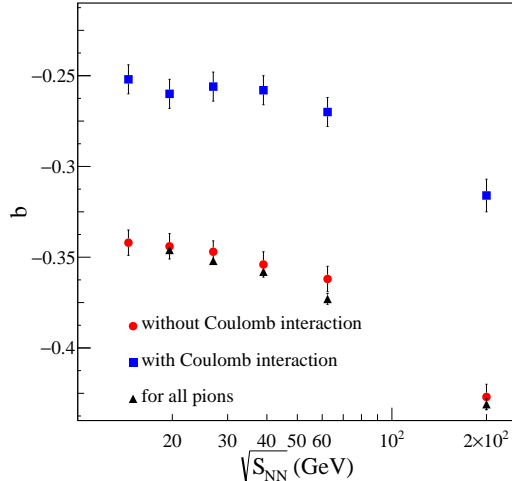


Figure 5. Collision energy dependence of parameter b .

4. The single-particle space-momentum angle distribution

In HBT research, the correlation function is often approximated by the on-shell momenta[31, 32]. So the correlation can also be written as[33]

$$C(\mathbf{q}, \mathbf{K}) \approx 1 + \frac{|\int d^4x S(x, K)) e^{i\mathbf{q}\cdot\mathbf{x}}|^2}{|\int d^4x S(x, K)|^2} \equiv 1 + | < e^{i\mathbf{q}\cdot\mathbf{x}} > |^2, \quad (5)$$

where $K_0 = E_K = \sqrt{(m^2 + |\mathbf{K}|^2)}$, $\mathbf{q} = \mathbf{p}_1 - \mathbf{p}_2$, then we get

$$e^{i\mathbf{q}\cdot\mathbf{x}} = \exp[i(\mathbf{p}_1 \cdot \mathbf{x} - \mathbf{p}_2 \cdot \mathbf{x})], \quad (6)$$

for the single-particle, we have already defined the angle $\Delta\varphi$ which is between the momentum direction and space direction, then we define two more angles,

$$\cos(\Delta\alpha) = \frac{\mathbf{p}_2 \cdot \mathbf{x}_1}{|\mathbf{p}_2| |\mathbf{x}_1|}, \quad (7)$$

$$\cos(\Delta\beta) = \frac{\mathbf{p}_1 \cdot \mathbf{p}_2}{|\mathbf{p}_1| |\mathbf{p}_2|}, \quad (8)$$

where $\Delta\alpha$ is the angle between the momentum direction and radius direction for two particles, and $\Delta\beta$ is the angle between the momentum directions for two particles. Then that

$$e^{i\mathbf{q}\cdot\mathbf{x}} \approx \exp \left[\frac{i}{2} (|\mathbf{K}| |x| \cos(\Delta\varphi) - |\mathbf{K}| |x| \cos(\Delta\alpha)) \right], \quad (9)$$

the $\Delta\alpha$ angle is not independent, its values are related to the $\Delta\beta$ and the $\Delta\varphi$, $\Delta\alpha = f(\Delta\varphi, \Delta\beta)$, so the correlation function can be written as

$$C(\mathbf{K}, \Delta\varphi, \Delta\beta) \approx 1 + \left| \left\langle \exp \left[\frac{i}{2} |\mathbf{K}| |\mathbf{x}| [\cos(\Delta\varphi) - \cos(f(\Delta\varphi, \Delta\beta))] \right] \right\rangle \right|^2. \quad (10)$$

When we calculate the HBT correlation function, we need to limit the values of momentum difference, $|\mathbf{q}| < q_{\max}$. If we choose the pair particles in one transverse momentum section, and because we focus on the mid-rapidity range, so the pair momenta are also screened, $k_{\min} < |\mathbf{K}| < k_{\max}$. In the same time, the angle $\Delta\beta$ is also limited, $\cos(\Delta\beta) > \frac{2k_{\min}^2}{k_{\min}^2 + q_{\max}^2} - 1$. So the $\Delta\beta$ values are related to the $|\mathbf{K}|$ values and the interaction between the particles. The $\Delta\varphi$ distribution can affect the HBT correlation and the HBT radii. And our research is focused on the transverse plane, so we discuss the connection between the $\Delta\theta$ distribution and R_s .

For a source, the collective flow is created by the expansion, and the transverse flow velocity are different at different layers of the source, which leads to different normalized $\Delta\theta$ distributions, as shown in Figure 6. N and N_R are the particle numbers in each bin, and N_R is obtained with the random \mathbf{p} and \mathbf{r} particles. The normalization process is using the $\cos(\Delta\theta)$ distribution divided by the random $\cos(\Delta\theta)$ distribution, and we let $\sum N = \sum N_R$. The particles with lower transverse momenta are closer to $N/N_R = 1$, this phenomenon indicates the source is approaching a random freeze-out source. While

with higher flow velocities, the distributions are closer to $\cos(\Delta\theta) = 1$, and it means the particles tend to freeze out along the radius direction. And for the particles that locate at 8-9 and 11-12 fm, their $\langle v_T \rangle$ values are closer, so they have similar normalized $\Delta\theta$ distributions.

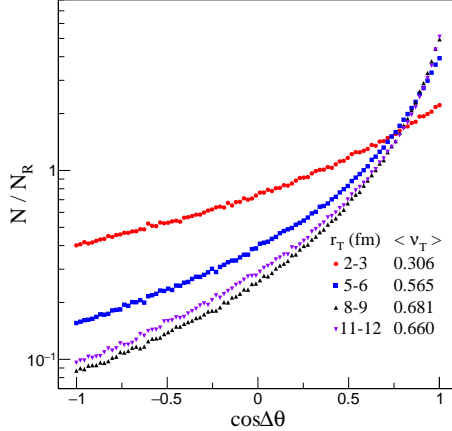


Figure 6. The normalized $\Delta\theta$ distributions in different transverse radii, π^+ particles are generated by the string melting AMPT model for the Au+Au collisions at $\sqrt{S_{NN}} = 62.4$ GeV/c.

Furthermore, for the particles with different transverse momenta P_T , they correspond to the parts of the whole source. And the particles with higher P_T , the part sources have bigger collective flow, as shown in Figure 7. The $\langle v_T \rangle$ increase with r_T inside of the source, and at the outside of the source, $\langle v_T \rangle$ almost becomes a constant. So the sizes of part sources are changing with the P_T .

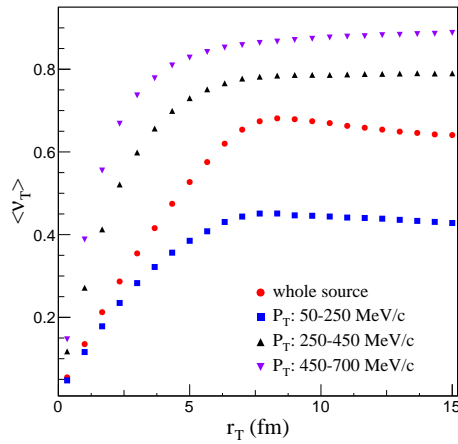


Figure 7. The transverse flow velocities for the transverse radii in different transverse momenta, π^+ particles are generated by the string melting AMPT model for the Au+Au collisions at $\sqrt{S_{NN}} = 62.4$ GeV/c.

The particles that freeze out from the source are always along with the collective flow, and the flow is different at different locations in the source, meanwhile the $\Delta\theta$ is related to the flow, so different $\Delta\theta$ have different freeze-out sources, as shown in Figure 8, for the π^+ particles that have large $\Delta\theta$ angles, their freeze-out directions are reversed to the space directions. And they have a small freeze-out source, which indicates they are almost freezing out from the center of the whole π^+ source. And those π^+ particles freeze out directions are perpendicular to the space directions have a bigger source, as shown in Figure 8(b). While in Figure 8(c), for the π^+ whose momentum directions along to the space directions, their freeze-out source has a ring shape, and has the biggest number density. So for this p_T section, most of π^+ particles freeze out from the shell, and the closer to the center of the source, the higher the probability of producing large $\Delta\theta$ angle particles. The normalized $\cos(\Delta\theta)$ distribution consists of a series of $\Delta\theta$ angles, so it corresponds to the source which is the superposition of partial sources. Therefore, the distribution is related to the HBT radius R_s .

If there is no correlation between the space and momentum, it will break the relation between $\Delta\theta$ and the source, and the differences of the normalized $\cos(\Delta\theta)$ distributions will disappear. Then the $\Delta\theta$ angle will be completely random, as shown in Figure 9. The normalized "no x-p correlation" distribution becomes a line, and the same in other K_T sections.

In Figure 9, we disrupt the space and the momentum correlation in each collision event. For example, original data are x_1p_1 and x_2p_2 , and after the disruption, they are x_1p_2 and x_2p_1 . This is a rough but effective method, and it can change the correlation between the space and the momentum, which means the particles can freeze out from the source in any direction. Then we calculate the HBT radius R_s , as shown in Figure 10.

The results show that the phenomenon of transverse dependence of R_s for "no x-p correlation" is almost disappeared. The R_s values for "no x-p correlation" are closer to each other, it is because they have the same normalized $\cos(\Delta\theta)$ distribution. And this method destroys the physical process, there will be fluctuations in calculating the correlation function, which leads to the emergence of the big error bars.

Moreover, we can build a numerical connection between the normalized $\cos(\Delta\theta)$ distribution and HBT radius R_s . We discuss the Coulomb interaction only for the HBT analysis, the two conditions are used the same string melting AMPT data, so they have the same normalized $\cos(\Delta\theta)$ distribution for different K_T regions. To describe the normalized $\cos(\Delta\theta)$ distributions, we introduce the fit functions

$$f = 0.002 \exp \left\{ c_1 \exp \left[c_2 \cos(\Delta\theta) \right] \right\}. \quad (11)$$

The value 0.002 is settled by us to get the good fitting results, and this value is a little bigger than our last work, in which we used center collision events and treated three kinds of pions as one. This value is most related to the proportion of the π^+ pairs whose freeze-out directions have big differences. It means this proportion for π^+ pairs is a little higher than our previous work, so the collective flow velocities of π^+ are a little smaller

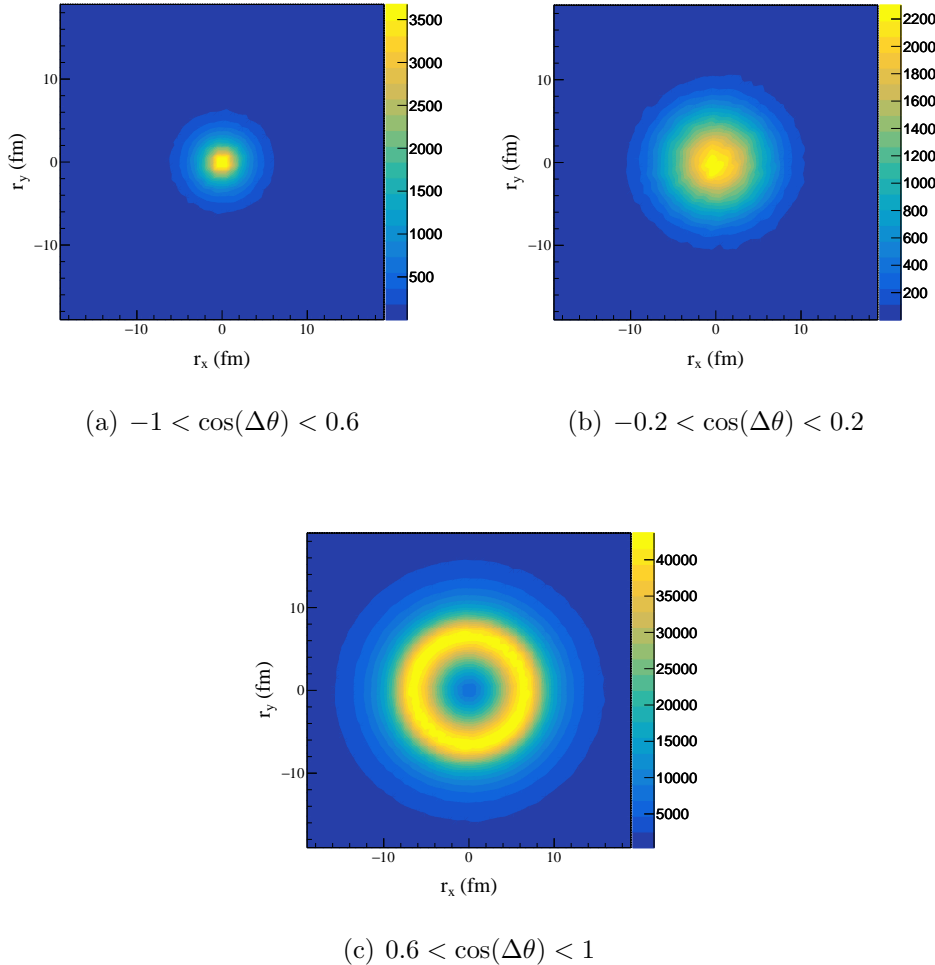


Figure 8. The freeze-out π^+ sources in different $\cos(\Delta\theta)$ sections. The particles are generated by the string melting AMPT model for the Au+Au collisions at $\sqrt{S_{NN}} = 62.4$ GeV, and the p_T range is 250–450 MeV/c.

than the velocities for all the pions. This is because the π^0 have a smaller mass than the π^+ and π^- . c_1 and c_2 are the fit parameters that we needed to fulfill the connection. For we change the settled value, these parameters change a lot than our previous work. Also, change the fit results in the next analysis, so the distributions are related to the kinds of particles. Then we fit them with

$$c_1 = k_1 \exp \left[-6 \times \left(\frac{K_T}{1000} \right)^2 \right] + j_1, \quad (12)$$

$$c_2 = k_2 \exp \left[-4.5 \times \left(\frac{K_T}{1000} \right)^2 \right] + j_2, \quad (13)$$

where -6 and -4.5 were chosen by us to obtain good fitting results, k and j are fit parameters. k_1 and j_1 are related the lowest proportion and the changing range of the proportion for the $\cos(\Delta\theta) = 0$ particles. k_2 and j_2 are related the lowest strength and the changing range of the strength for the normalized $\cos(\Delta\theta)$ distribution approach to

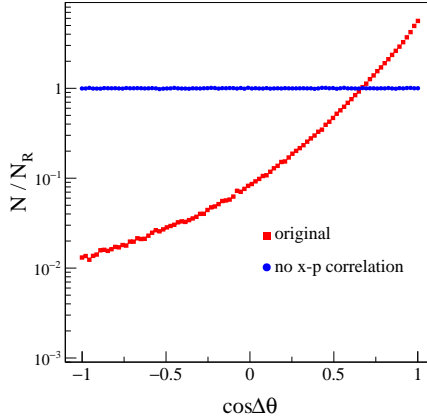


Figure 9. The original distribution and the no x-p correlation distribution at $\sqrt{S_{NN}} = 62.4$ GeV, and the K_T range is 325–375 MeV/c.

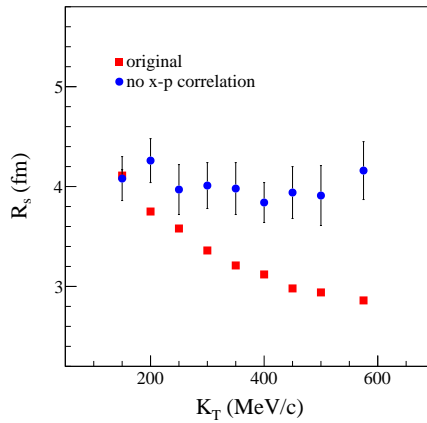


Figure 10. The original R_s and no x-p correlation R_s at $\sqrt{S_{NN}} = 62.4$ GeV.

$$\cos(\Delta\theta) = 1.$$

For making the collision energies add to this connection, we plot the parameter b , obtained from the transverse momentum dependence of R_s , as the functions of the parameters k and j , as shown in Figure 11. The changing patterns indicate parameter b has an extremum, we set $b_1 = -0.2$ for the situation without the Coulomb interaction, and $b_2 = -0.3$ for considering the Coulomb interaction. We use the functions to fit these patterns, they are

$$b(k_m) = \mu_{m1}|k_m|^{\mu_{m2}} + b_n, \quad (14)$$

$$b(j_m) = \nu_{m1}|j_m|^{\nu_{m2}} + b_n, \quad (15)$$

where $m = 1$ or 2 , it is for distinguishing the parameters of c_1 or c_2 . Also $n = 1$ or 2 , then 1 is for the situation without the Coulomb interaction, and 2 means the Coulomb interaction. μ and ν are fit parameters, and the fitting results are shown in Table 1.

The results show, the Coulomb interaction have influence on these fit parameters, it can decrease $|\mu_{m1}|$ and $|\nu_{m1}|$, and increase $|\mu_{m2}|$ and $|\nu_{m2}|$. It is caused by the changing of the differences of b values. And the differences of b values between the two situations are increasing with increasing the collision energies. Compared with our previous work, the changing patterns are different, so these numerical connections are also related to the kinds of particles.

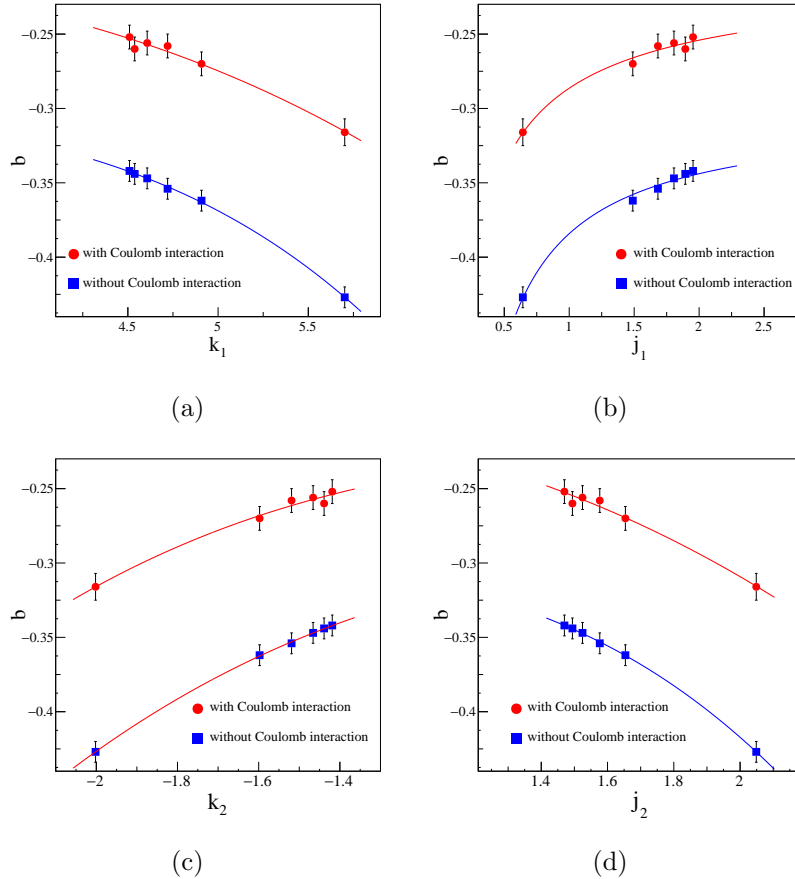


Figure 11. The numerical connections between the strength of the transverse momentum dependence of R_s and the parameters related to the normalized $\cos(\Delta\theta)$ distribution, the lines are fit lines.

With these fit functions and parameters, the numerical connections between the normalized $\cos(\Delta\theta)$ distribution and the strength of the transverse momentum dependence of R_s have been built. With a series of R_s data in different K_T regions, the distributions as a function of K_T can be estimated. The Coulomb interaction influences the calculation of the HBT radii and the b values. And the particles we analyzed are freeze-out particles, there is no interaction between them, so the single-particle space-momentum angle distributions are the same to each other, no matter with and without Coulomb interaction. The changing pattern for these two situations are similar, it is reflected in these little close fit results, while the differences of them are caused by the Coulomb interaction, which has bigger inhibition for the strength of the transverse

Table 1. Fit results for parameters μ and ν

		$n = 1$	$n = 2$
m=1	μ_{11}	-0.0004 ± 0.0003	-0.00004 ± 0.00003
	μ_{12}	3.3 ± 0.5	4.7 ± 0.4
	ν_{11}	-0.086 ± 0.004	-0.084 ± 0.003
	ν_{12}	-0.68 ± 0.09	-0.94 ± 0.08
	μ_{21}	-0.024 ± 0.003	-0.014 ± 0.003
	μ_{22}	2.3 ± 0.3	3.2 ± 0.3
m=2	ν_{21}	-0.021 ± 0.004	-0.012 ± 0.002
	ν_{22}	2.4 ± 0.3	3.3 ± 0.3

momentum dependence of R_s at high collision energies, and this phenomenon is also shown in Figure 5. With further research, the chosen values and fit results can be improved by adding more collision energies and more accurate fits.

Conclusions

With the string melting AMPT model, we calculate the HBT radius R_s for π^+ in two situations, with and without Coulomb interaction. The results indicate the Coulomb interaction can decrease the R_s values and inhibits the transverse momentum dependence of R_s . We show the transverse flow can affect the normalized $\cos(\Delta\theta)$ distributions, and the flow changes with the location of the source, which leads to the particles with bigger $\Delta\theta$ angles tending to freeze out from the inner of the source. We also present the normalized $\cos(\Delta\theta)$ distributions can influence the transverse momentum dependence of R_s by disrupting the space and the momentum correlation. The π^+ are already frozen out, the Coulomb interaction has no influence on the space and momentum of π^+ , so there are the same normalized $\cos(\Delta\theta)$ distributions for the two situations. While the inhibition of the transverse momentum dependence of R_s caused by Coulomb interaction, leads to the changing of the fit results. And different kinds of particles have different numerical connections. With these numerical connections, we can get more information about the final stage of the Au+Au collision at the freeze-out time by the HBT analysis. With more collision energies and more accurate fits, the numerical connection can be improved. There are anomalies near the CEP, it may change this connection, so the improvement connection may be a probe to detect the CEP. And the Coulomb interaction can weaken the strength of the transverse momentum dependence of R_s , it may also weaken the sensitivity of this probe.

References

- [1] Hanbury Brown R and Twiss R 1956 *Nature* **178** 1046–1048
- [2] Goldhaber G, Goldhaber S, Lee W and Pais A 1960 *Phys. Rev.* **120**(1) 300–312
- [3] Lisa M A, Pratt S, Soltz R and Wiedemann U 2005 *Annu. Rev. Nucl. Part. Sci.* **55** 357–402
- [4] Heinz U and Jacak B V 1999 *Annu. Rev. Nucl. Part. Sci.* **49** 529–579

- [5] Wiedemann U A and Heinz U 1999 *Phys. Rep.* **319** 145 – 230 ISSN 0370-1573
- [6] Kittel W 2001 *Acta. Phys. Pol. B* **32** 3927
- [7] Alexander G 2003 *Rep. Prog. Phys.* **66** 481–522
- [8] Annan Lisa M, Pratt S, Soltz R and Wiedemann U 2005 *Annu. Rev. Nucl. Part. Sci.* **55** 357–402
- [9] Adams J, Aggarwal M, Ahammed Z, *et al.* (STAR Collaboration) 2005 *Nuclear Physics A* **757** 102–183
- [10] Adcox K, Adler S, Afanasiev S *et al.* (PHENIX Collaboration) 2005 *Nuclear Physics A* **757** 184–283
- [11] Borsanyi S, Fodor Z, Hoelbling C *et al.* (Wuppertal-Budapest Collaboration) 2010 *J. High Energy Phys.* **09** 073
- [12] Hatta Y and Ikeda T 2003 *Phys. Rev. D* **67**(1) 014028
- [13] Stephanov M, Rajagopal K and Shuryak E 1998 *Phys. Rev. Lett.* **81**(22) 4816–4819
- [14] Aggarwal M M *et al.* (STAR Collaboration) 2010 (*Preprint* 1007.2613)
- [15] Stephanov M A 2005 *Int. J. Mod. Phys. A* **20** 4387–4392
- [16] Lacey R A, Ajitanand N N, Alexander J M, Chung P, Jia J, Taranenko A and Danielewicz P 2007 (*Preprint* 0708.3512)
- [17] Lacey R A 2015 *Phys. Rev. Lett.* **114**(14) 142301
- [18] Pratt S 1984 *Phys. Rev. Lett.* **53**(13) 1219–1221
- [19] Wiedemann U A, Scotto P and Heinz U 1996 *Phys. Rev. C* **53**(2) 918–931
- [20] Yang H, Feng Q, Ren Y, Zhang J and Huo L 2020 *Chin. Phys. C* **44** 054105
- [21] Yang H, Feng Q, Ren Y, Zhang J and Huo L 2021 *Chin. Phys. C* **45** 104102
- [22] Lin Z W, Ko C M, Li B A, Zhang B and Pal S 2005 *Phys. Rev. C* **72**(6) 064901
- [23] Shan L Q, Wu F J, Liu J L, Feng Q C, Wang Q S, Zhang J B and Huo L 2009 *J. Phys. G-Nucl. Part. Phys.* **36** 115102
- [24] Zhang Y, Zhang J, Liu J and Huo L 2015 *Phys. Rev. C* **92**(1) 014909
- [25] Zhang Y, Zhang J, Chen T, Liu D and Chao Y 2017 *Phys. Rev. C* **96**(4) 044914
- [26] Lin Z w, Ko C M and Pal S 2002 *Phys. Rev. Lett.* **89**(15) 152301
- [27] Alexander G 2003 *Rep. Prog. Phys.* **66** 481–522
- [28] Adams J, Aggarwal M M, Ahammed Z *et al.* (STAR Collaboration) 2005 *Phys. Rev. C* **71**(4) 044906
- [29] Pratt S 2006 Crab version 3.0 <https://web.pa.msu.edu/people/pratts/freecodes/crab/home.html>
- [30] Aamodt K, Quintana A A, Adamová D *et al.* 2011 *Phys. Lett. B* **696** 328 – 337
- [31] Bertsch G F, Danielewicz P and Herrmann M 1994 *Phys. Rev. C* **49**(1) 442–451
- [32] Pratt S, Csörgő T and Zimányi J 1990 *Phys. Rev. C* **42**(6) 2646–2652
- [33] Chapman S, Scotto P and Heinz U W 1995 *Acta Phys. Hung. A* **1** 1–31